PCCP

PAPER

View Article Online
View Journal | View Issue

Cite this: *Phys. Chem. Chem. Phys.*, 2020, **22**, 26806

Electron spectroscopy and dynamics of HBr around the Br $1s^{-1}$ threshold†

Nacer Boudjemia,*[a] Kari Jänkälä,[a] Ralph Püttner,[b] Tatiana Marchenko,[cd] Oksana Travnikova,[cd] Renaud Guillemin,[cd] Loïc Journel,[cd] Iyas Ismail,[cd] Dimitris Koulentianos,‡[ce] Satoshi Kosugi,[gh] Yoshiro Azuma,[gh] Minna Patanen,[a] Marko Huttula,[a] Denis Céolin,[d] Maria Novella Piancastelli[cf] and Marc Simon[cd]

Received 10th September 2020,
Accepted 12th November 2020

DOI: 10.1039/d0cp04787b

rsc.li/pccp

A comprehensive electron spectroscopic study combined with partial electron yield measurements around the Br 1s ionization threshold of HBr at ≅13.482 keV is reported. In detail, the Br $1s^{-1}$ X-ray absorption spectrum, the $1s^{-1}$ photoelectron spectrum as well as the normal and resonant KLL Auger spectra are presented. Moreover, the L-shell Auger spectra measured with photon energies below and above the Br $1s^{-1}$ ionization energy as well as on top of the Br $1s^{-1}\sigma^*$ resonance are shown. The latter two Auger spectra represent the second step of the decay cascade subsequent to producing a Br $1s^{-1}$ core hole. The measurements provide information on the electron and nuclear dynamics of deep core-excited states of HBr on the femtosecond timescale. From the different spectra the lifetime broadening of the Br $1s^{-1}$ single core-hole state as well as of the Br($2s^{-2}$,$2s^{-1}2p^{-1}$,$2p^{-2}$) double core-hole states are extracted and discussed. The slope of the strongly dissociative HBr $2p^{-2}\sigma^*$ potential energy curve is found to be about −13.60 eV $Å^{-1}$. The interpretation of the experimental data, and in particular the assignment of the spectral features in the KLL and L-shell Auger spectra, is supported by relativistic calculations for HBr molecule and atomic Br.

1 Introduction

Availability and opportunity of combining a high-photon-energy source with a high-resolution hemispherical energy analyzer, such as the hard X-ray photoelectron spectroscopy (HAXPES) end station at GALAXIES beamline,[1,2] SOLEIL synchrotron, has opened new avenues for the investigation of photoionization and photoexcitation dynamics.[3,4] A similar spectroscopic set-up has been developed also recently at SPring-8 in Japan by Oura *et al.*[5] These new possibilities allow, for example, studying nuclear dynamics on the sub-femtosecond time scale for K-shell ionization and relaxation of heavy element containing molecules *via* normal Auger, absorption-like and resonant Auger (RAS) spectroscopies. In the present work we concentrate on the Br K-edge (≅13.48 keV) in the HBr molecule.

Electronic states related to the Br K-edge excitation have been a subject of investigation in the past. As an example, a study on the relative intensities and energies of Br KLL Auger spectrum was reported by Erman *et al.*[6] Photoabsorption spectra of Br_2 around the K-edge were measured and supported with *ab initio* theory by Kincaid *et al.*[7] In that work the first high-resolution extended X-ray-absorption fine structure (EXAFS) spectrum of Br around the K-edge was presented. Other studies were carried out by D'Angelo *et al.*,[8] on the double-electron excitation channels at the Br K-edge of HBr and Br_2. Recently, non-dipole asymmetries of Br K-shell photoelectrons have been reported by Southworth *et al.*[9] In addition, photoabsorption spectrum of gaseous HBr up to 50 eV above the K-edge has been studied in ref. 10.

In isolated molecules, excitation of an electron from the core to the lowest unoccupied molecular orbital (LUMO) can induce fast nuclear dynamics if the state has a steep dissociative potential energy surface. Core-excited states are also highly

[a] *Nano and Molecular Systems Research Unit, University of Oulu, P.O. Box 3000, 90014 Oulu, Finland. E-mail: nacer.boudjemia@oulu.fi*
[b] *Fachbereich Physik Freie Universität Berlin, Arnimallee 14, D-14195 Berlin, Germany*
[c] *Sorbonne Université, CNRS, Laboratoire de Chimie Physique-Matière et Rayonnement, LCPMR, F-75005, Paris, France*
[d] *Synchrotron SOLEIL, L'Orme des Merisiers, Saint-Aubin, BP 48, F-91192 Gif-sur-Yvettes Cedex, France*
[e] *Department of Physics, University of Gothenburg, Origovägen 6B, SE-412 96 Gothenburg, Sweden*
[f] *Department of Physics and Astronomy, Uppsala University, SE-75120 Uppsala, Sweden*
[g] *Department of Materials and Life Sciences, Sophia University, Tokyo 102-8554, Japan*
[h] *Department of Physics, Tokyo Gakugei University, 4-1-1 Nukuikita-machi, Koganei, Tokyo 184-8501, Japan*

† CCDC. For crystallographic data in CIF or other electronic format see DOI: 10.1039/d0cp04787b

‡ Present address: Chemical Sciences and Engineering Division, Argonne National Laboratory, 9700 S Cass Avenue, Lemont, IL 60439, USA.

unstable electronically, characterized by a very short lifetime, ranging typically from a few femtoseconds to even tens of attoseconds. They decay rapidly by emitting photons or electrons *via* radiative or non-radiative processes, respectively. Thus, nuclear dynamics and the decay of the core-excited state can be in competition, and the photon energy dependence of these processes has been utilised to probe ultra-fast nuclear dynamics using the so-called core-hole clock spectroscopy (CHCS).[11–16] The most relevant techniques for CHCS studies are resonant inelastic X-rays scattering (RIXS) and resonant Auger spectroscopy (RAS). A detailed description and a comparison of RIXS and RAS techniques are reported by Marchenko *et al.* in ref. 17.

Studies of nuclear dynamics of deep core orbitals of molecules containing heavy atoms are quite scarce. This is due to limited availability of high-resolution X-ray sources that can handle gaseous samples. If an electron in hydrogen halide molecules, HX (X = F, Cl, Br or I), is promoted to LUMO, the molecule is put into a strongly dissociative state because of LUMO's antibonding character. The electronic lifetime of core-excited states can be comparable to molecular dissociation time, occurring on a femtosecond timescale. Therefore, the excited electronic state can decay when the system is already, or becoming, atomic-like, and the study of the electronic decay can yield information on nuclear dynamics. In a pioneering study of HBr with angle-resolved photoelectron spectroscopy conducted by Morin *et al.*,[11] observation of large and sharp resonant Auger peaks showed direct experimental evidence of repulsive character of $Br(3d^{-1}\sigma^*)$ state and a competition between atomic and molecular resonant Auger decay. Similar results have been reported later by Aksela *et al.* in the case of the HCl molecule,[18,19] showing evidence of ultrafast dissociation following excitation to the σ^* orbital. In addition, similar behavior has been reported for H_2O, O_2, NH_3, SF_6, CF_4, and CH_3Cl molecules, see *e.g.*.[20–23] However, to our knowledge, dynamics involving a very deep K-edge above 10 keV have not been performed so far. It is important to note that such a deep core hole results in a dissociation of the molecule in the timescale of several femtoseconds. However, in the present work we focus on the first two decay steps which occur on a timescale of less than 1 fs. For this timescale, and based on the results presented below, 0.1 Å was estimated as an upper limit for the internuclear distance elongation, which implies that dissociation should take place during the subsequent decay processes. Despite the small bond elongation we observe indication of the initiated dissociation process.

In this article we study the photoabsorption spectrum measured in partial electron yield mode as a function of photon energy including the 1s $\rightarrow$ σ^* resonance, the Br 1s photoelectron spectrum and the subsequent $HBr^{1+} \rightarrow HBr^{2+}$ and $HBr^{2+} \rightarrow HBr^{3+}$ Auger decay spectra. The recorded resonant Auger spectra as a function of photon energy provide insight into the molecular dynamics following $HBr(1s^{-1})$ excitation. The extracted information is related to the line narrowing below the core-hole-lifetime broadening and to the anomalous dispersion of $2p^{-2}\sigma^*$ spectral lines showing an S-like dispersion as a function of photon energy. The $2p^{-2}$ double-core-hole (DCH) lifetime is determined to be about 2 times shorter in comparison to $2p^{-1}$ single-core-hole (SCH) lifetime using a simplified form of the Kramers–Heisenberg cross section equation,[17] and the value is confirmed by the results from a fit of KLL normal Auger electron lines. The slope of the potential energy curve (PEC) of $2p^{-2}\sigma^*$ states populated from the Auger relaxation of $1s^{-1}\sigma^*$ states is estimated to be -13.60 eV Å^{-1}. In addition, relaxation of the Rydberg state $1s^{-1}5p$ is studied.

The analysis of experimental photoelectron and Auger spectra are supported by relativistic molecular Dirac–Fock and atomic multi-configuration calculations for HBr and Br, respectively. The calculations are in good agreement with the experimental results.

2 Experiment

The experiments were carried out at the GALAXIES beamline,[1,2] of the SOLEIL Synchrotron in Saint Aubin close to Paris, France. The data were recorded with a Scienta EW4000 hemispherical deflection energy analyser by applying different modes. The electron spectrometer was mounted in perpendicular position to the beam and parallel to the linear polarization of the synchrotron light, with a gas cell mounted at the bottom of the main chamber. The photoelectron and KLL Auger spectra were measured with photon energies of 13.8 and 13.6 keV, respectively. The $HBr^{1+} \rightarrow HBr^{2+} \rightarrow HBr^{3+}$ Auger spectra ($HBr^{0+} \rightarrow HBr^{1+} \rightarrow HBr^{2+}$ at σ^* resonance) were recorded using photon energies of 13.55, 2.3 and 13.47 keV. These values are for above and below the HBr 1s ionization threshold, and on the top of the HBr $1s^{-1}\sigma^*$ resonance, respectively. The resonant KLL Auger 2D-map and the X-ray absorption measurements were carried out in partial electron yield mode, scanning the photon energy from 13 467 to 13 483 eV with a step of 0.5 eV, and a kinetic energy window of 10 160–10 320 eV.

During the measurements the target pressure in the main chamber was about 2×10^{-5} mbar. The energy resolution of the electron energy analyzer was about 1 eV with a pass energy of 500 eV and a slit width of 800 μm. Based on the fit of a Ar $1s^{-1}$ photoelectron spectrum the photon bandwidth is estimated to be 2.5 eV at the photon energy of 13.8 keV. The kinetic-energy scale of the electron-energy analyzer was calibrated using the Ar KLL and KLM Auger spectra.[24,25] The kinetic energy scale of the spectrometer in the range of 9700–10 300 eV was also calibrated with Ar KLL and KLM Auger spectra, due to lack of more appropriate calibration lines. The photon energy was calibrated using the Ar 1s photoelectron line.[25]

3 Calculations

The molecular calculations were carried out using the DIRAC code[26] to obtain the $HBr(1s^{-1})$ ionization energy and $HBr(1s^{-1}\sigma^*)$ excitation energies within the Δ-SCF framework using the Dyall's triple-ξ basis set.[27] A H–Br bond length of 1.41 Å in the ground state was taken as a fixed value from literature.[28] The molecular

calculations were carried out using the relativistic Dirac–Coulomb Hamiltonian and correcting the values further with Breit and quantum electrodynamics (QED) corrections from atomic GRASP2k code,[29] as discussed in ref. 30.

In addition, relativistic atomic calculations within a configuration–interaction Dirac–Fock framework using the GRASP2K code[29] were carried out. The inherently relativistic calculations included also Breit interaction and QED corrections (self-energy, vacuum polarization) as subsequent perturbations.

The Auger spectra subsequent to K and L-orbital photoionization, photoexcitation, KL-emission and KLL-Auger decay were simulated by including all relevant energetically allowed final states obtainable from the ground state configuration of atomic Br. The photoionization cross-sections and radiative transition rates were calculated in a dipole approximation with a length gauge using PHOTO and REOS components of the RATIP package,[31] respectively.

Auger decay rates were calculated using the FAC code,[32] which uses the same theoretical framework as GRASP2K and provides about the same state energies. The FAC code was used for calculating the Auger rates due to its reliability and considerably shorter execution times in comparison to GRASP2K and RATIP.

4 The photoabsorption spectrum around the Br $1s^{-1}$ threshold

Fig. 1 shows the absorption spectrum of HBr in the photon energy region of 13467.5 to 13 489 eV measured using the partial electron yield method. A fit to the spectrum consists of two peaks indicated by solid subspectra, namely Br $1s^{-1}\sigma^*$ and Br $1s^{-1}5p$, and an arctan-function which accounts for higher Rydberg states and the continuum cross section. Note that the higher molecular states are assigned to *n*p Rydberg states since for 3d absorption they can be classified in Rydberg series,[33,34] *i.e.* they experience the HBr^+ ion as an almost point-like charge distribution; a more detailed argumentation why Br 1s and Br^+ absorption spectra are closely related to each other are given below.

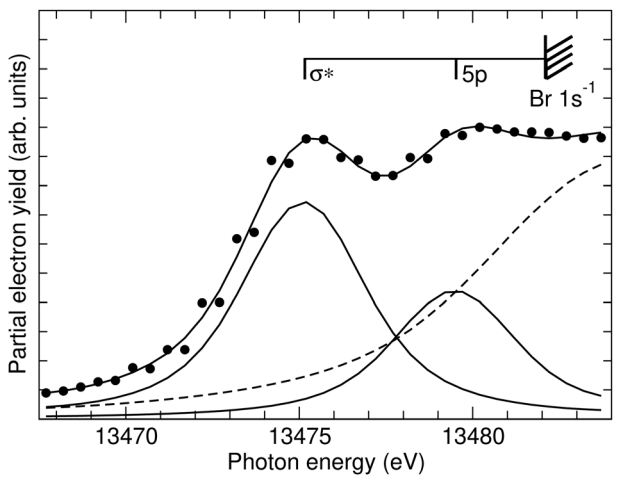

Fig. 1 Br $1s^{-1}$ absorption spectrum measured by recording the resonant Auger partial electron yield in the KLL energy window of 10 160 to 10 320 eV. The solid line through the data points represent the fit result. The solid subspectra indicate the individual lines and the dashed subspectrum the background. The bar diagram above the spectrum shows the assignment.

For the two distinct spectral features the same lifetime broadening, represented by a Lorentzian function, is used resulting in a value of Γ = 2.66(34) eV full width at half maximum (FWHM). The spectral features are also convoluted with a Gaussian width of 2.50 eV in order to account for the photon bandwidth; this value is obtained from fitting the Ar $1s^{-1}$ photoelectron line recorded at a photon energy in the same range and it has an estimated error of ±100 meV. The Br $1s^{-1}\sigma^*$ transition was also convoluted with a second Gaussian in order to simulate broadening due to the dissociative character of the excited state. In fits where the respective parameter was free it turned out that ≅1 eV can be considered as an upper limit. Since this value agrees with the respective broadening observed in the Br $3d^{-1}$ photoion yield spectrum[33,34] it was used as fixed parameter in the fits performed to obtain the Br $1s^{-1}$ lifetime broadening. Note that molecular properties like potential energy curves, geometry, or term values mainly depend upon the valence-shell structure, but not upon a particular core hole; this is reflected in the equivalent-core or Z + 1 approximation. As a consequence, in core-level photoabsorption the final-state orbital is most important for these properties. Therefore we can expect similar values for *e.g.* the Br $1s^{-1}\sigma^*$ and the Br $3d^{-1}\sigma^*$ states. Following the same argument, only one Lorentzian is used for the Br $1s^{-1}5p$ state as no vibrational excitations are observed for the Br $3d^{-1}5p$ states.[33,34] The two peaks labelled as Br $1s^{-1}\sigma^*$ and Br $1s^{-1}5p$ are found at $h\nu$ = 13475.1(1) eV and $h\nu$ = 13479.5(2) eV, respectively. From the latter value and the term values of the Br $3d^{-1}5p$ resonances[33,34] the threshold energy can be estimated to be $h\nu$ = 13482.1(3) eV. Note that the statistical error bars refer to relative distances. In addition, the energies are subject to an additional error of ≅2 eV due to the calibration of the energy scale.

Table 1 summarises experimental and calculated Br $1s^{-1}$ binding energy and Br $1s^{-1}\sigma$*/4p/5p excitation energies for molecular HBr as well as atomic Br. The molecular calculations carried out with the Dirac code are in good agreement with the values extracted from the experiment. In addition, the experimental values are supported by the atomic calculations carried out using the GARSP2K code for neutral atomic Br and for Kr-like anion (not shown here). The results show an interesting behaviour, namely that the experimental Br $1s^{-1}$ binding energy value agrees much better with the value obtained for neutral atomic Br rather than Br^-. This can be understood from the electronegativity of both Br and H atoms. The electronegativity values of Br and H are 2.96 and 2.2, respectively. The values are given in dimensionless Pauling scale.[35] Therefore the difference between the two electronegativity values is 0.76, which defines a mildly polar covalent bond type, where the Br atom has only a slight negative charge $Br^{\delta-}$. This explains why Br appears as ''Br-like'' in the HBr molecule. In addition, the calculated atomic Br $1s^{-1}5p$ excitation energy is found to be in agreement with the experimental energy value obtained for HBr $1s^{-1}5p$. This due to the fact that the 5p orbital in the HBr molecule has a strong Rydberg character, as reflected also on KLL Auger spectra, see Section 6.2.

Table 1 Experimental and calculated $1s^{-1}$ and $1s^{-1} \rightarrow \sigma^*/4p/5p$ energies of atomic Br and HBr molecule (in eV). The theoretical calculation were carried out using DIRAC and GRASP2K code. All experimental energies are additionally subject to an error of ≅2 eV due to the calibration of the energy scale

	Bromine $1s^{-1}$		Bromine $1s \rightarrow \sigma^*/4p$		Bromine $1s \rightarrow 5p$	
	HBr	Br	HBr	Br	HBr	Br
Dirac	13480.90	—	13475.50	—	13478.81	—
GRASP2K	—	13481.65	—	13468.68	—	13479.13
Experiment	13482.1(3)	—	13475.1(1)	—	13479.5(2)	—

5 The Br $1s^{-1}$ photoelectron spectrum

The Br $1s^{-1}$ photoelectron spectrum measured using a photon energy of $h\nu$ = 13.8 keV is displayed in Fig. 2. The red line through the data points represents the results of a fit analysis, which was performed to extract a second value for the Br $1s^{-1}$ core-hole lifetime width. In the fit analysis it has been taken into account that the Br $1s^{-1}$ core hole decays, according to the present calculations, see below, by 61% by X-ray emission, by 31% by KLL Auger decay and by 8% by KLY Auger decay, with the major contribution by KLM Auger decay; note that throughout this publication we use X = L, M, N and Y = M, N. Because of this, Br $1s^{-1}$ main peak is described with three contributions, namely a Lorentzian lineshape (black solid subspectrum) for the X-ray emission as well as a post-collision interaction (PCI) lineshape[36] for both the KLL (blue solid subspectrum) and KLM (orange solid subspectrum) contributions. The intensities are weighted according to the above given percentages and all three contributions are described with the same parameter for the lifetime broadening. Moreover, to describe the PCI lineshapes, an average kinetic energies of 10 and 11.55 keV for the KLL and KLM Auger transitions respectively were used. Finally, four Gaussians were employed to describe the shake-up satellite structures; they are indicated by the dashed black subspectrum. The lineshapes were convoluted with a Gaussian of 2.7 eV to account for the photon bandwidth of 2.5 eV and the spectrometer resolution of 1.0 eV. To estimate the error bars, the Gaussian lineshape describing the experimental resolution was varied by ±0.1 eV.

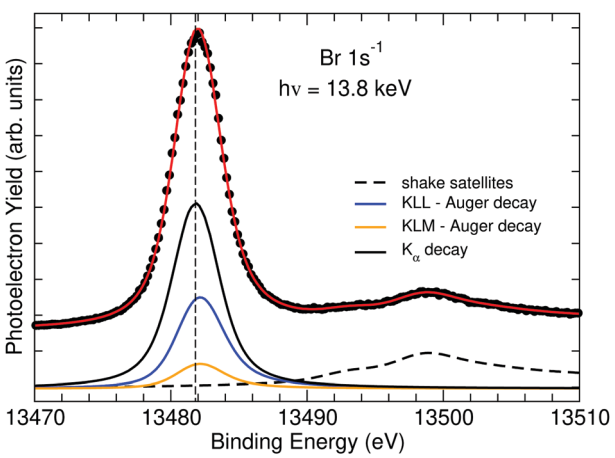

Fig. 2 The Br $1s^{-1}$ photoelectron spectrum of HBr including the shake-up and shake-off region measured using a photon energy of $h\nu$ = 13.8 keV. The red solid line through the data points indicates the fit result and the subspectra different contributions. For details, see text.

The thin vertical dashed line serves as guide to the eye to stress that the three contributions to the main line show different line profiles due to PCI shifts and distortions. From the fit we obtained $\Gamma_{1s^{-1}}$ = 2.37(10) eV, which we combined with $\Gamma_{1s^{-1}}$ = 2.66(34) eV from the absorption spectrum to $\Gamma_{1s^{-1},exp}$ = 2.40(12) eV. This value is slightly lower than the theoretical result of $\Gamma_{1s^{-1},theo}$ = 2.52 eV reported in ref. 37. Moreover, the obtained value is 0.25 eV lower than the value of $\Gamma_{1s^{-1}}$ = 2.65(14) eV recently obtained for Kr,[38] which agrees well with the difference of 0.23 eV calculated by Krause and Oliver.[37]

In the energy region around 13 500 eV shake-up satellite structures are visible. The spectral structures match, beside the larger lifetime broadening and, therefore, the less pronounced structures, quite well the satellite structures of the Cl $2p^{-1}$ spectrum of HCl.[39] In the latter spectrum the satellites are explained with transitions originating to the 4σ, 5σ, and 2π valence orbitals,[39] which suggests that the similar structures in HBr are due to shake-up transitions to the valence orbitals 7σ, 8σ, and 4π. A detailed discussion of the shake structures in HBr is beyond the scope of this article. However, as will be discussed below, their presence is relevant for the interpretation of the Br KLL Auger spectrum.

6 The Auger spectra

6.1 The Br KLL normal Auger decay

Fig. 3 shows the Br KLL Auger spectrum of HBr subsequent to HBr $1s^{-1}$ photoionization at $h\nu$ = 13.6 keV measured with an experimental resolution of 1 eV, together with relativistic calculation carried out for neutral atomic-Br. The small shift seen in the energy positions is most likely due to the average energy level scheme used in the calculation. The calculated spectrum is built-up from the singly ionised Br^+ ($1s^{-1}$) state, that undergo a KLL Auger relaxation to Br^{2+}, giving rise to $2s^{-2}$, $2s^{-1}2p^{-1}$ and $2p^{-2}$ final states. This allows an assignment of the diagram lines in full agreement with literature.[6] Note, that transitions to the $2p^{-2}(^3P_J)$ final states are forbidden in pure LS coupling and are absent in lighter atoms such as neon.[40] The presence of the final states $2p^{-2}(^3P_{0,2})$ in the Auger spectrum indicates, together with the splitting of the transitions to the final states $2s^{-1}2p^{-1}(^3P_0,^3P_1,^3P_2)$, significant spin–orbit interaction for the Br 2p shell. Note, that the transitions to the final states $2p^{-2}(^3P_0)$ and $2p^{-2}(^3P_2)$ gain intensity from configuration interaction with the final states of the same value of J, namely $2p^{-2}(^1S_0)$ and $2p^{-2}(^1D_2)$. In contrast to this, the closest state for

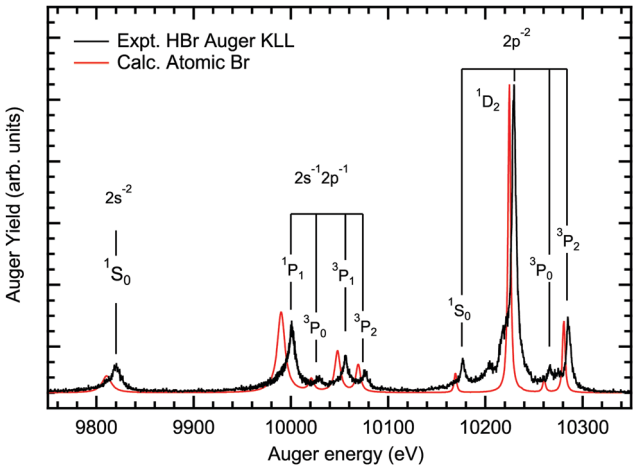

Fig. 3 The experimental and calculated Br KLL Auger spectrum of HBr including the assignment of the diagram lines.

$2p^{-2}(^3P_1)$ that can mix with it is $2s^{-1}2p^{-1}(^3P_1)$, which is about 200 eV higher in energy, which makes mixing negligible.[40]

To our knowledge, the present spectrum is the first Br KLL Auger spectrum reported in the literature since the work of Erman and coworkers published in 1965.[6] In their work, the $1s^{-1}$ core hole in a ^{79}Br atom was formed by an electron-capture decay of ^{79}Kr and the experiment had a resolution of 10 eV, which is rather modest by modern standards.

The Br KLL Auger transitions were fitted in order to extract the lifetime broadenings of the Br $2p^{-2}$, $2s^{-1}2p^{-1}$ and $2s^{-2}$ double core-hole (DCH) states. In the analysis it was assumed that all DCH states of the Br $2p^{-2}$ configurations show the same lifetime broadening. For the $2s^{-1}2p^{-1}$ configurations the present calculations suggest different lifetimes for the individual states. In particular, for the $2s^{-1}2p^{-1}(^3P)$ states similar lifetime broadenings are calculated, while for the $2s^{-1}2p^{-1}(^1P)$ state a significantly larger value was obtained. Following these results we assumed in the fit analysis the same lifetime broadening for the $2s^{-1}2p^{-1}(^3P)$ states and a different one for the $2s^{-1}2p^{-1}(^1P)$ state.

The upper panel of Fig. 4 shows the Br $1s^{-1} \rightarrow 2p^{-2}$ Auger transitions. All the four diagram lines Br $1s^{-1} \rightarrow 2p^{-2}(^1S_0,^1D_2,^3P_0,^3P_2)$ show a slight asymmetry with a tail towards higher kinetic energies. This is due to PCI and therefore the lines are fitted with PCI lineshapes[36] and convoluted with a Gaussian of 1 eV FWHM in order to account for the spectrometer resolution. This procedure resulted in a linewidth of $\Gamma = 5.12(10)$ eV. By subtracting the lifetime broadening of the $1s^{-1}$ core hole, $\Gamma_{1s^{-1}} = 2.40(12)$ eV, we obtain $\Gamma_{2p^{-2}} = 2.72(22)$ eV. Note that in the fit analysis the kinetic energy of the photoelectron was treated as a free parameter resulting in $E_{kin,PE} \cong 340$ eV, which is much larger than the actual value of $\cong$120 eV. This is due to the fact that we approximated the line with one PCI-lineshape of 5.12(10) eV width. A correct treatment of the spectral feature would be a PCI-lineshape with the linewidth of the Br $1s^{-1}$ photoline convoluted with a Lorentzian of the linewidth of the Br $2p^{-2}$ double core hole final states;[41] however, this is not

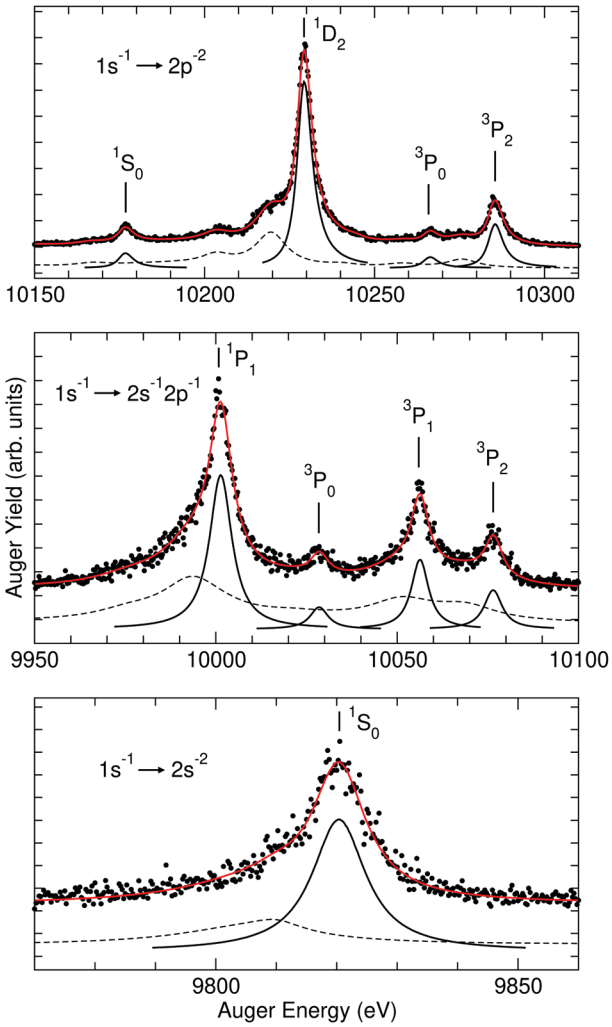

Fig. 4 Details of the Br KLL Auger spectrum including the fit results. The upper panel shows the Br $1s^{-1} \rightarrow 2p^{-2}$ Auger transitions, the middle panel the Br $1s^{-1} \rightarrow 2s^{-1}2p^{-1}$ transitions, and the lower panel the Br $1s^{-1} \rightarrow 2s^{-2}$ transitions. The red solid line through the data points represents the fit result. The black solid subspectra indicate the fitted diagram lines and the black dashed-lines the background consisting predominantly of Auger decays caused by shake satellites during the photoionization process. For details, see text.

implemented in the fit program and the additional error caused by this approximation is small compared to the uncertainty in the lifetime broadening of the Br $1s^{-1}$ core hole.

The Br $1s^{-1} \rightarrow 2s^{-1}2p^{-1}(^1P_1,^3P_0,^3P_1,^3P_2)$ Auger lines are shown in the middle panel of Fig. 3. As mentioned above, in the fit two different parameters for the linewidths were used, namely one for the Br $1s^{-1} \rightarrow 2s^{-1}2p^{-1}(^1P_1)$ transition and one for the Br $1s^{-1} \rightarrow 2s^{-1}2p^{-1}(^3P)$ transitions. Since for the latter transitions, the lifetime broadenings are found to be slightly larger than Br $1s^{-1} \rightarrow 2p^{-2}(^1S_0,^1D_2,^3P_0,^3P_2)$, both were fitted with Lorentzian and PCI lineshapes. However, the values for the intensities and widths resulted in practically identical χ^2-values and the parameters turned out to differ only within the error bars. Moreover, in the fit using a PCI lineshape for the photoelectron, a kinetic energy of $E_{kin,PE} \cong 750$ eV was

obtained; this indicates a rather Lorentzian-like lineshape. As the main difference between the two approaches, for the Br $1s^{-1} \rightarrow 2s^{-1}2p^{-1}(^3P)$ transitions the fit using PCI lineshapes provided 0.40(3) eV lower Auger energies than the fit using symmetric Lorentzian lineshapes. We consider this value a guide value for the size of systematic errors due to the simplified description of the lineshapes, see above.

For the Br $1s^{-1} \rightarrow 2s^{-1}2p^{-1}(^1P_1)$ transition, only a Lorentzian lineshape was used. In detail, for the Br $1s^{-1} \rightarrow 2s^{-1}2p^{-1}(^1P_1)$ transition a total width of 7.35(60) eV and for the Br $1s^{-1} \rightarrow 2s^{-1}2p^{-1}(^3P)$ transitions a total width of 5.56(50) eV were obtained. From these values the double core hole lifetime widths of $\Gamma_{2s^{-1}2p^{-1}(^1P_1)}$ = 4.95(72) eV and $\Gamma_{2s^{-1}2p^{-1}(^3P)}$ = 3.16(62) eV were derived. For the Br $1s^{-1} \rightarrow 2s^{-2}(^1S_0)$ Auger transition displayed in the lower panel of Fig. 3 a width of 10.60(21) eV is obtained, resulting in a lifetime broadening of $\Gamma_{2s^{-2}}$ = 8.20(33) eV.

In the present work the Br^{2+} DCH lifetime widths were also calculated by assuming an Auger relaxation of Br^{2+} initial states to Br^{3+} final states. From the calculations the following widths are obtained: $\Gamma_{2p^{-2}}(^1S_0,^1D_2,^3P_{0,2})$ = 2.72 eV, $\Gamma_{2s^{-1}2p^{-1}}(^1P_1,^3P_{0,1,2})$ = 9.37, 5.94, 6.57 and 5.33 eV, respectively, and $\Gamma_{2s-2}(^1S_0)$ = 11.58 eV. For the state $2p^{-2}(^1S_0,^1D_2,^3P_0,^3P_2)$ perfect agreement with the experiment is found. For the states with holes in the 2s level, the theoretical results show clearly the same tendency, but they are systematically too large.

In the following we compare the L-shell DCH lifetime broadenings with the values of the single core-hole (SCH) states calculated by Krause and Oliver,[37] which are $\Gamma_{2s^{-1}}$ = 4.11 eV, $\Gamma_{2p_{1/2}{}^{-1}}$ = 1.21 eV, and $\Gamma_{2p_{3/2}{}^{-1}}$ = 1.08 eV. The result provides DCH/SCH linewidth ratios of 2.00(0.08) for the 2s orbital and 2.39(21) for the $\Gamma_{2p_{3/2}{}^{-1}}$ = 1.08 orbital. The value for the 2s orbital agrees within the error bars with the expected ratio of 2 for deeper core holes.[42] The value of the 2p orbital is somewhat larger, however, still smaller than the ratios close to three obtained for shallow core levels, namely Ne 1s with a ratio of 2.9(1)[42] and Ar 2p with a ratio of 2.8(2).[43] For the $2s^{-1}2p^{-1}$ DCH the situation is more complex. The sum of the $2s^{-1}$ and the $2p^{-1}$ lifetime broadenings of $\cong$5.25 eV agrees within the error bars with the value of $\Gamma_{2s^{-1}2p^{-1}(^1P_1)}$ = 4.95(72) eV for the singlet state. It is, however, significantly larger than the value of $\Gamma_{2s^{-1}2p^{-1}(^3P)}$ = 3.16(62) eV for the triplet states. This can at least partially be understood by the fact that the $L_1L_{2,3}Y$ Coster–Kronig Auger probability of the $2s^{-1}$ vacancy is significantly reduced due to the presence of the $2p^{-1}$ hole. We want to point out that in a naive picture the spin of the holes are parallel in the triplet states and antiparallel in the singlet state. As a result, in the triplet states only two $2s^{-1}$ electrons can fill the 2s hole without spin–flip, while in the singlet state three 2p electrons are available for filling the 2s hole; this might explain the larger linewidth for transitions to the latter state. For argon it has also been observed that the lifetime broadening of the $1s^{-1}2p^{-1}$ DCH states is smaller than the sum of the broadening of the single core-hole states[44] and it was also explained with a reduced Auger rate due to a reduced number of 2p electrons which are involved in the main Auger decay channel.

In all panels of Fig. 4 the dashed solid black lines indicate the background, which predominantly consists of features related to the Auger decay of photoionization shake-up satellite states. Practically for all diagram lines a shake satellite structure shifted by about 10 eV to lower kinetic energies can be observed. A similar observation has been made, for example, for the KLL Auger spectrum of H_2S[45] and Ar[46] where the corresponding satellites could unambiguously be assigned to Auger decays of the satellite lines in the photoelectron spectrum. Shake processes during the Auger decay were found at kinetic energies which are lower by $\cong$15 to 30 eV with respect to the diagram lines and they turned out to have considerably lower intensities. This suggests to assign the spectral features found at kinetic energies about 10 eV below those of the diagram lines as Auger processes of the photoelectron satellites presented in Fig. 2 and the spectral feature at $\cong$10 205 eV to a shake process during the Br $1s^{-1} \rightarrow 2p^{-2}(^1D_2)$ Auger decay.

Additional results of the fit are accurate values for the energy splitting and relative intensity ratios between the different diagram lines. These results are summarised in Table 2, together with the present theoretical results. The numbers in parentheses indicate the statistical error bars. Generally, a good agreement is observed. In more detail, the theoretical splitting between the states is somewhat larger than the experimental values. For the relative intensities a good agreement is observed, with the exception of the $Br^{-1} \rightarrow 2s^{-2}$ transition showing an experimental values 3 times larger than the theoretical one. The fit model is, however, limited by the description of the shake structures in the Auger spectrum, since the exact contributions of these structures to the spectrum are unknown. We estimate that this can lead to systematic errors for the intensity ratio in the order of 10% of the given relative value, while the energy positions are essentially unaffected.

6.2 The HBr KLL resonant Auger decay

In Fig. 5(a) the resonant KLL Auger spectra as a function of photon energy is recorded as a 2D-map, where the intensities are represented by the color scale. The 2D-map is measured in

Table 2 Summary of the fit and calculation results of the Br KLL Auger transitions. Given are the experimental and theoretical Auger energies, E_{Auger} as well as the experimental and theoretical relative Auger energies, E_{rel}, and the relative Auger intensities. For both quantities the values are given relative to the Br $1s^{-1} \rightarrow 2p^{-2}(^1D_2)$ transition. The numbers in parentheses indicate the statistical error bars. For systematic error bars, see text. The experimental Auger energies are additionally subject to an error of $\cong$2 eV due to the calibration of the energy scale

	E_{Auger} (eV)		E_{rel} (eV)		Relative intensity (arb. units)	
Final state	Exp.	Calc.	Exp.	Calc.	Exp.	Calc.
$2p^{-2}(^3P_2)$	10285.1	10281	56.16(5)	56	0.23(1)	0.23
$2p^{-2}(^3P_0)$	10265.9	10260	37.04(13)	35	0.06(1)	0.04
$2p^{-2}(^1D_2)$	10228.9	10225	0	0	1.00	1.00
$2p^{-2}(^1S_0)$	10176.3	10169	-52.60(10)	−56	0.08(1)	0.06
$2p^{-1}2p^{-1}(^3P_2)$	10076.6	10069	−152.30(34)	-156	0.05(1)	0.09
$2p^{-1}2p^{-1}(^3P_1)$	10056.3	10048	−172.62(33)	−177	0.09(2)	0.13
$2p^{-1}2p^{-1}(^3P_0)$	10028.6	10021	−200.35(46)	−204	0.03(1)	0.04
$2p^{-1}2p^{-1}(^1P_1)$	10001.4	9990	−227.57(16)	−235	0.26(2)	0.26
$2s^{-2}(^1S_0)$	9820.4	9811	−408.54(20)	−414	0.16(1)	0.05

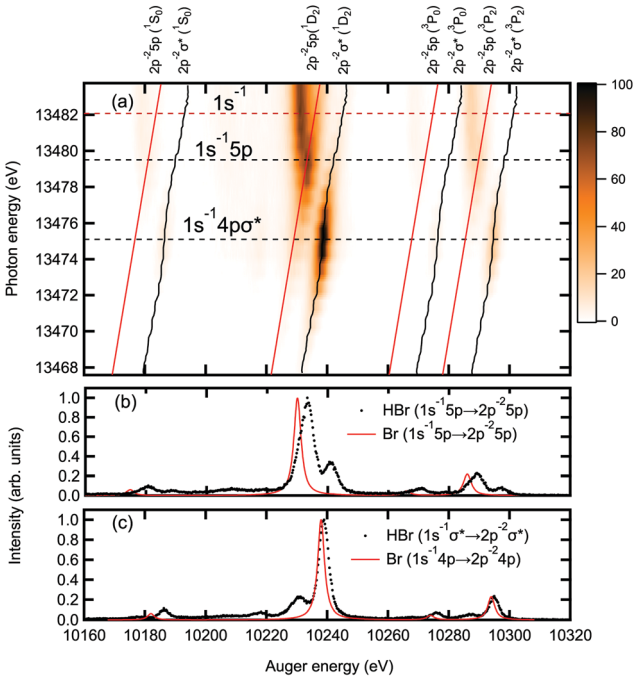

Fig. 5 The panel (a) shows a 2D-map of the resonant KLL Auger decay. The *x*-axis shows the Auger energies and the *y*-axis the photon energy used for excitation. An integration along the *x*-axis results in the absorption spectrum shown in Fig. 1. The intensities are shown in color scale. The two dashed horizontal black lines represent the resonance energies of $1s^{-1}\sigma^*$ and $1s^{-1}5p$, (compare to Fig. 1). The dashed horizontal red line represents the $1s^{-1}$ ionization threshold. The tilted vertical black solid lines with an S-shape at the $1s^{-1}\sigma^*$ resonance energy indicate the kinetic energy dispersion of the $2p^{-2}\sigma^*$ final state. The tilted vertical linear red solid lines indicate the kinetic energy dispersion of $2p^{-2}5p$ Rydberg states. In the lower panels (b) and (c) the experimental HBr and the calculated atomic Br KLL resonant Auger spectra measured and calculated on top of the $1s^{-1}5p$ and $1s^{-1}\sigma^*$ resonances are shown. The intensity maxima are set to 1.

the kinetic energy range of 10 160–10 320 eV with a step width of 0.25 eV and in the photon energy range of 13 467–13 484 eV with a step width of 0.5 eV. Using photons with energy lower than the 1s binding energy of 13 482 eV, a predominantly resonant Auger decay of the type

$$\gamma + HBr \rightarrow HBr^*(1s^{-1}V) \rightarrow HBr^* + (2p^{-2}V) + e_{KLL}^- \quad (1)$$

takes place. Note that V refers to unoccupied valence and Rydberg orbitals. Above the HBr $1s^{-1}$ ionization threshold the normal Auger decay described by

$$\gamma + HBr \rightarrow HBr^+(1s^{-1}) + e_{ph}^- \rightarrow HBr^{2+}(2p^{-2}) + e_{KLL}^- \quad (2)$$

dominates. Note that the dispersion of the resonant Auger lines does not end at the $1s^{-1}$ ionization threshold, but continues above the threshold as reported for example in ref. 47 and 48, where the dispersive lines are followed directly by non-dispersive lines following ι-shape due to the PCI effect, see *e.g.* the KLL Auger spectra of argon[41] and HCl.[48] Based on PCI lineshape simulations using the formula given by Armen *et al.*[36] the ι-like shape of the normal Auger transitions in a 2D-map is expected to be stretched over a photon energy range of at least some 10 eV so that the measured 2 eV above threshold are too small to observe this effect.

The vertical tilted solid black and red lines show the kinetic energy dispersion of the $2p^{-2}\sigma^*$ and $2p^{-2}5p$ final states, respectively. Around the lower horizontal dashed line representing the resonance energy of the Br $1s^{-1}\sigma^*$ excitation, the black line exhibits an S-shape behavior. This S-shape indicates nuclear motion in the Br $1s^{-1}\sigma^*$ state due to the dissociative character of the σ* orbital. In this case, part of the photon energy is spent for the movement of nuclei and is not available for the emitted Auger electron. Note that these S-shaped features are not pronounced in Fig. 5(a). For the $2p^{-2}(^1D_2)\sigma^*$ final state it can be seen more clearly in the panel (a) of Fig. 6. For the $2p^{-2}5$ p Auger final states mainly populated *via* $1s^{-1}5p$, a tilted linear red line in the upper panel of the Fig. 5(a) indicates a normal (linear) kinetic energy dispersion. This can be understood by assuming that the states are non-dissociative,[48] see Section 4.1.

The calculated resonant KLL Auger spectra subsequent to $1s^{-1}5p$ and $1s^{-1}4p$ resonant excitations in the Br atom are shown as red lines in panels (b) and (c) of Fig. 5, respectively. The resonant KLL Auger final states are built-up by assuming an excitation of an electron from 1s to 4p, to mimic the excitation of the electron from the 1s orbital to the σ* (LUMO), and an excitation from 1s to 5p, to mimic the transition to the higher Rydberg orbitals in the HBr molecule. These states undergo resonant Auger spectator decay, mainly to the $2p^{-2}(^3P_2,^3P_0,^1D_2,^1S_0)np$ final states.

The simulated spectra shown in the panels (b) and (c) of Fig. 5 are in a good agreement with the experiment in terms of the intensity features. The kinetic energy of the $1s^{-1}5p \rightarrow 2p^{-2}5p$ resonant Auger transitions displayed in panel 5(b) shows a mismatch between experiment and theory comparable

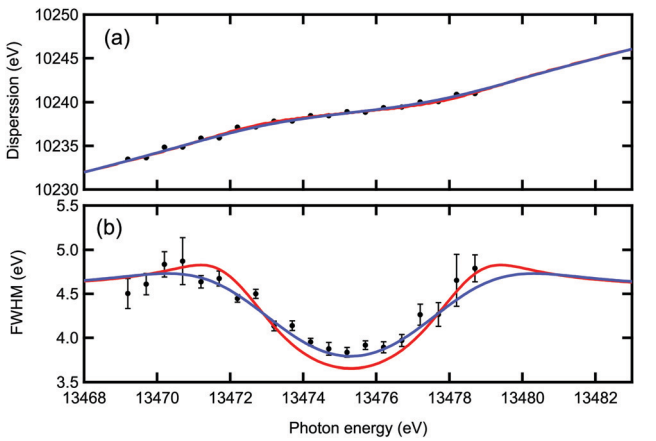

Fig. 6 The kinetic energy dispersion (a) with exchanged axes in comparison to Fig. 5(a) and the full width at half maximum (FWHM) (b) of the $1s^{-1}\sigma^* \rightarrow 2p^{-2}(^1D_2)\sigma^*$ transition as a function of the incident photon energy in the energy range of the $1s^{-1}\sigma^*$ resonance. Error bars are from the fits of the experimental spectra using Voigt profiles. The red lines are the results of fit using eqn (3) and the blue lines are the results of the convolution of the eqn (3) with an additional Gaussian of 2.7 eV to simulate the experimental resolution.

to the one for the $1s^{-1} \rightarrow 2p^{-2}$ normal Auger transitions visible in Fig. 3. This similar energy mismatch confirms that the 5p orbital can be simulated by atomic calculations, *i.e.* it has a strong Rydberg character. Contrary to this, the agreement of the energy positions of the experimental $1s^{-1}\sigma^{\star} \rightarrow 2p^{-2}\sigma^{\star}$ and the theoretical $1s^{-1}4p \rightarrow 2p^{-2}4p$ resonant Auger transitions displayed in panel 5(c) is much better. We consider this finding coincidental and refer to the fact that an excitation to the molecular valence orbital $\sigma^{\star}$ is compared with an atomic excitation; this difference compensates by accident the energy mismatch inherent to the $1s^{-1} \rightarrow 2p^{-2}$ transition. Note that the theoretical $1s^{-1}4p \rightarrow 2p^{-2}4p$ transition represents the Auger decay at long bond distances, *i.e.* after dissociation, while the bond elongation during the Br $1s^{-1}$ core-hole lifetime is practically zero. The spectral features in panel (b) of Fig. 5 show an asymmetric lineshape and a larger width compared to the calculated Br atomic spectrum. The reason for this is the presence of a number of unresolved $1s^{-1}5p \rightarrow 2p^{-2}np$ shake-up Auger transitions with $n > 5$. Such a behaviour has been observed also for Xe in ref. 49. Note that the shake processes during Auger decay have not been taken into account in the calculations.

The black points in Fig. 6(a) and (b) display the anomalous kinetic energy dispersion and the linewidth of the $1s^{-1}\sigma^{\star} \rightarrow 2p^{-2}(^1D_2)\sigma^{\star}$ transition, respectively. The data points have been obtained by fitting the line with a Voigt profile where both Gaussian and Lorentzian widths were free parameters. More specifically, the data were fitted using a simplified form of the generalized Kramers–Heisenberg formula.[50] The equation is frequently used to describe RIXS cross sections in the case of dissociative intermediate states. The simplified form for the present case is extracted from ref. 17 as

$$\sigma(\omega,\omega') \propto \int_{-\Delta U_f}^{\infty} d\varepsilon \exp\left(-\frac{\varepsilon^2}{\Delta_f^2}\right) L(\omega - \omega_{co} - \varepsilon, \Gamma_c) \times L(\omega - \omega' - \omega_{fo} - \varepsilon, \Gamma_f). \quad (3)$$

Fig. (7) indicates the relation between the different quantities used in the eqn (3), in which ω and ω' are the incident photon energy and the kinetic energy of the resonant Auger electron, respectively. Moreover, $\varepsilon = E_f - \Delta U_f$ is the nuclear kinetic energy at $r \rightarrow \infty$, E_f, reduced by the potential energy difference $\Delta U_f = U_f(r_e) - U_f(r \rightarrow \infty)$ with $U_f(r_e)$ and $U_f(r \rightarrow \infty)$ being the potential energy of the final state at the equilibrium distance r_e and at $r \rightarrow \infty$, respectively. Note that $\varepsilon = 0$ for excitations at the equilibrium distance, and is negative for excitations at larger internuclear distances. $\Delta_f = \mathscr{F}_{fo}a_0$, is the Franck–Condon factor, where $\mathscr{F}_{fo}$ is the absolute value of the gradient of the PEC of the dissociative final state at r_e and a_0 is the width of the Franck–Condon distribution between the ground and the final state. ω_{co} is the energy of the vertical transition from the ground (o) to the intermediate state (c) and ω_{fo} is the energy of the vertical transition from ground state (o) to the final state (f). $\Gamma_{c,f}$ are the lifetime broadenings of the intermediate and final states.

In the present case the cross section reduces to a product of a Gaussian function representing the bound-free FC factors and

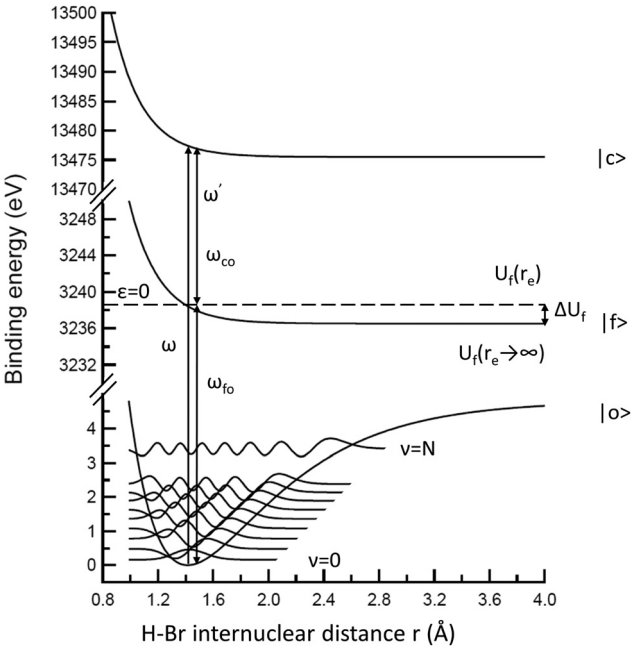

Fig. 7 Rough schematic diagram indicating the different used parameters in the eqn (3).

two Lorentzian functions that account for the core-excited intermediate and final states lifetimes Γ_c and Γ_f, respectively. Note that eqn (3) needs to be further convoluted with a Gaussian describing the instrumental resolution for direct comparison with the experiment. Eqn (3) is obtained in the Franck–Condon and Born–Oppenheimer approximations. Furthermore, in the present case both final and intermediate states are strongly dissociative, but, due to the short lifetime of the 1s core-excited state, ~280 as, nuclear propagation in the intermediate state has been neglected. For more details, see ref. 17.

The fits were performed by fixing the parameters as follows: Γ_c = 2.40(12) eV, ω_0 = 2648.975 cm^{-1} (which gives a_0 = 0.11 Å from $a_0 = [\hbar/\mu\omega_0]^{1/2}$), μ = 0.99 amu, r_e = 1.41 Å, ω_{co} = 13475.5 eV and ω_{fo} = 3236.5 eV. Γ_f and $\mathscr{F}_{fo}$ were set as free parameters.

From the fits, the value of Γ_f = 2.50(5) eV as the DCH lifetime for $Br(2p^{-2})$ can be found. The obtained value for the $2p^{-2}\sigma^{\star}$ final states agrees within the error bars with the one obtained for the $2p^{-2}$ final states of $\Gamma_{2p^{-2}}$ = 2.72(22) eV. The value for the $2p^{-2}\sigma^{\star}$ final states gives a DCH/SCH ratio of 2.23 by taking the Br $2p^{-1}$ SCH width to be 1.12 eV[37,51] as an average from $2p_{1/2}$ and $2p_{3/2}$ SCH lifetimes. The obtained ratio from the fitting method is thus in good agreement with the $\tau_{2p^{-1}} \sim 2\tau_{2p^{-2}}$ ratio extracted from the normal KLL Auger spectrum, see above.

Concerning the Frank–Condon (FC) factor Δ_f a value of 1.5 eV has been obtained, giving rise to $F_{fo}(2p^{-2})$ = −13.60(10) eV $Å^{-1}$ as a slope of the $Br(2p^{-2}\sigma^{\star})$ PEC. The reflected behaviour on the kinetic energy peak dispersion and the line narrowing in the Fig. 6 is a manifestation of nuclear dynamic effects across the $1s^{-1}\sigma^{\star}$ resonance, where a part of the photon energy is transferred to the nuclei in the HBr molecule leading to the elongation and breaking of H–Br bond as stated above.

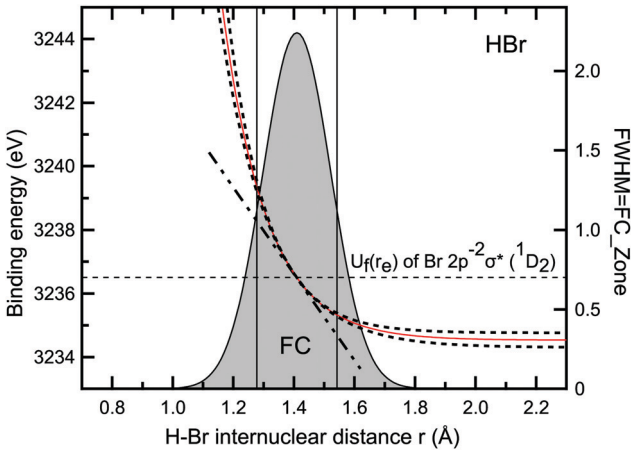

Fig. 8 PEC reconstructed from experimental data for Br $2p^{-2}(^1D_2)\sigma^*$ DCH state reached by resonant Auger decay (red solid curve). The area between the two dashed curves corresponds to the uncertainty of 0.5 eV for the asymptotic PEC values calculated for atomic Br. The vertical lines mark the FC zone determined from FWHM of the fundamental vibrational wave function of HBr molecule at $r = r_e$. The black horizontal dashed line corresponds to the potential of Br $2p^{-2}\sigma^*(^1D_2)$ states at $r = r_e$, $U_f(r_e) \cong$ 3236.5 eV.

Fig. 8 shows the PEC of the $2p^{-2}\sigma^*$ state as a function of H-Br distance using the following equation from ref. 17, where the dissociative potential $U_f(r)$ can be described by an exponential shape

$$U_f(r) = \Delta U_f \exp\left[\left(\frac{-\mathscr{F}_{fo}}{\Delta U_f}\right)(r - r_e)\right] + U_f(r \to \infty). \quad (4)$$

Here, the value of $U_f(r_e) \cong$ 3236.5 eV is known from the experiment. For $U_f(r \to \infty)$ a value of $\cong$3234.6 eV is used. It is estimated as a sum of atomic Br $2p^{-2}4p(^1D_2)$ binding energy of 3230.8 eV (calculated using GRASP2K) and the experimental H–Br dissociation energy of about 3.8 eV.[52]

The PEC at the FC zone shows strong dissociative character for the $2p^{-2}\sigma^*$ states. The obtained slope value is reasonable in comparison to the slopes of $2p^{-2}\sigma^*$ PEC obtained for H–Cl and CH_3–Cl, where the values are −14.5 eV Å^{-1}[115] and −11.10(30) eV Å^{-1}[117] respectively.

6.3 L-shell Auger decay of HBr

Panels (a), (c) and (e) of Fig. 9 show the experimental Auger spectra of HBr in the electron kinetic energy range of 1000–1550 eV, *i.e.* the decay of L single core-holes formed by direct ionization or KL X-ray emission and LX double core-holes with X = L, M, N formed by KLX Auger decay or LLY (Y = M, N) Coster–Kronig decay. Consequently, the spectra comprise LYY, LX–XYY, and LY–XYY Auger decays. The Auger spectra are measured above (Fig. 9a) and below (Fig. 9c) the K-edge, as well as at the $1s^{-1}\sigma^*$ resonance (Fig. 9e). Panels (b), (d) and (f) show the corresponding theoretical spectra calculated for atomic Br. The Auger spectra are very similar to the respective spectra recorded from atomic Kr,[38,53,54] except for the fact that the Kr spectrum is shifted by $\cong$85 eV to higher kinetic energies. Therefore it is possible to identify the main features of the present spectra in more detail by comparison to Fig. 2 and Table 2 of ref. 38. The similarity is due to the fact that the studied Auger decay takes place between deep core orbitals, which causes the overall shape of the spectra to be similar between Br and Kr.

The above K-edge spectrum displayed in Fig. 9(a) and the resonant (spectator) Auger spectrum in Fig. 9(e) show very similar structure and differ only by an energy shift of the latter spectrum to higher kinetic energies by $\cong$10 eV. This is due to the fact that the L-shell holes are populated by the same pathways. Comparison of the spectra in panels (a) and (c) recorded above and below the K-edge, however, shows subtle differences in the peak intensities. Similar differences have been observed for atomic $1s^{-1}$ ionization spectra of Xe[55] and Kr[38] as well as in I $1s^{-1}$ ionization of CH_3I and CF_3I in ref. 56. These differences can be understood by different population pathways leading to the L-hole states by ionization below and above the $1s^{-1}$ threshold. In the following the pathways will be discussed in detail.

Using a photon energy below the HBr 1s ionization threshold, the L-hole states can be populated only by direct photoionization of $L_{1,2,3}$ orbitals. Thus the population of the initial states of Auger decay are described by the photoionization branching ratios of $L_{1,2,3}$ orbitals. Note that, $L_{2,3}$ states can in principle be populated by $L_1 \rightarrow L_{2,3}$ fluorescence decay. This channel is, however, negligible in comparison to the L_1XY Auger decay so that we can write

$$\gamma + Br \rightarrow Br^+(2s^{-1},2p^{-1}) + e_{ph} \quad (5)$$

The most prominent relaxation pathway of $Br^+(2s^{-1},2p^{-1})$ ionic states is LMY Auger decay, where Y = M, N, in the energy region under discussion. The Contribution of this path is displayed in panel 9(d) as the $Br^{1+} \rightarrow Br^{2+}$ subspectrum. In addition, $2s^{-1}$ and $2p_{1/2}{}^{-1}$ core hole states can decay *via* $L_1L_{2,3}Y$ and L_2L_3Y Coster–Kronig processes, respectively. The kinetic energy of Coster–Kronig Auger electrons is well below the currently studied energy range, but it leads to double-hole states where one of the holes is in the 2p orbital. These states can decay further by emitting an electron into the studied kinetic energy range, see below for the description 2p hole decay.

Using a photon energy above the HBr 1s ionization threshold or a photon energy around the HBr $1s^{-1}\sigma^*$ resonance leads predominantly to a hole in the K-shell. Above threshold, the probability for creating a K-hole is 86%, an L_1-hole is 8% and an $L_{2,3}$-hole is 6%. Eqn (6) shows the three K-hole decay paths that lead to one or two L-holes

$$\gamma + Br \begin{cases} \xrightarrow{\sim 86\%} Br^{1+}(1s^{-1}) + e_{ph} \\ \xrightarrow{\sim 8\%} Br^{1+}(2s^{-1}) + e_{ph} \\ \xrightarrow{\sim 6\%} Br^{1+}(2p^{-1}) + e_{ph} \end{cases} \quad (6)$$

$$Br^{1+}(1s^{-1}) \begin{cases} \xrightarrow{61\%} Br^{1+}(2p^{-1}) + \gamma_{K\alpha} \\ \xrightarrow{31\%} Br^{2+}(2s^{-2}, 2s^{-1}2p^{-1}, 2p^{-2}) + e_{KLL} \\ \xrightarrow{8\%} Br^{2+}(2s^{-1}2p^{-1})nl^{-1} + e_{KLY} \end{cases}$$

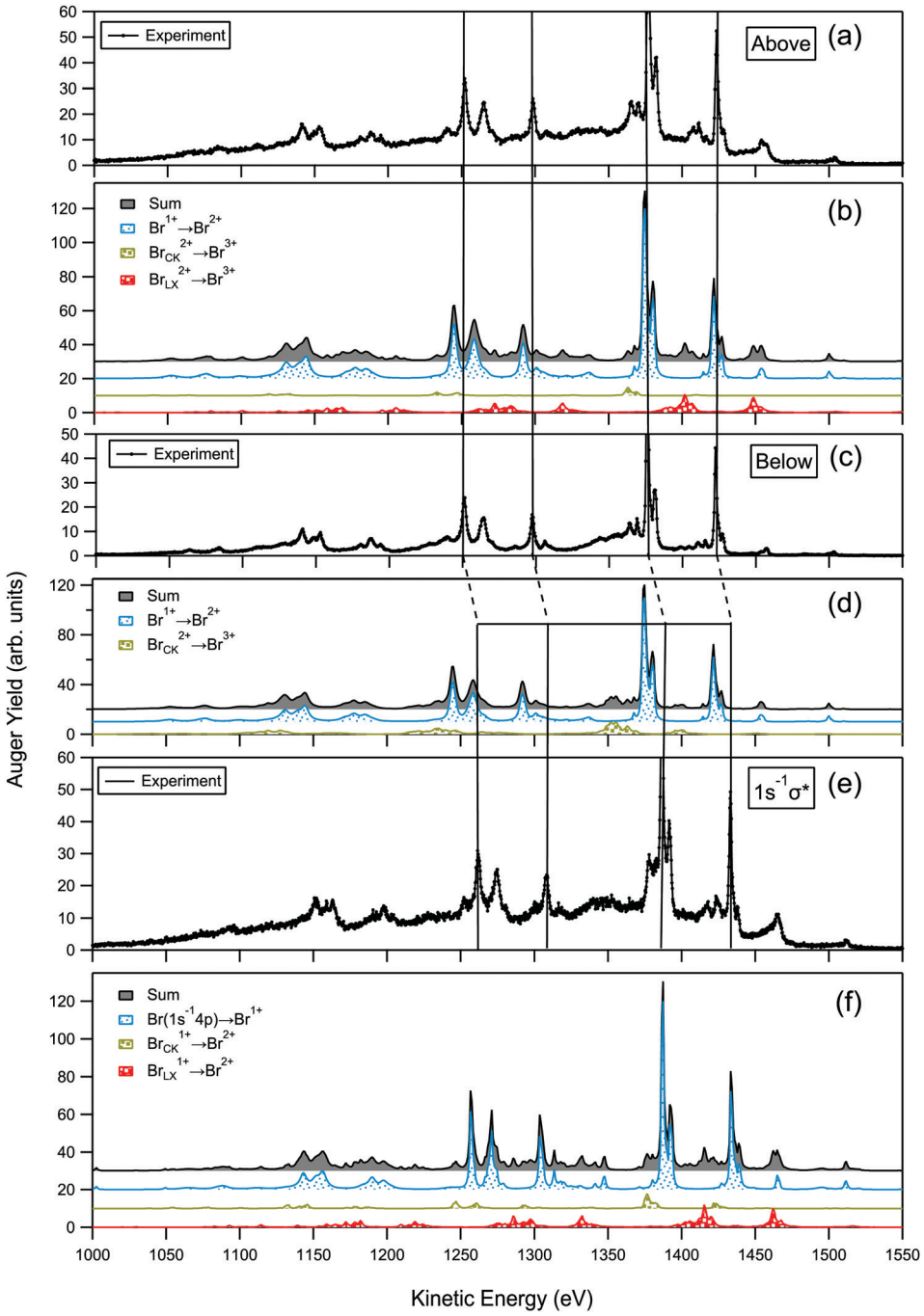

Fig. 9 The experimental Auger spectra with holes in the L-shell measured (a) at 13 550 eV, *i.e.* above the 1s ionization threshold, (c) at 2300 eV, *i.e.* below the 1s ionization threshold, and (e) at 13 475 eV, *i.e.* at the 1s → σ* resonance. The corresponding theoretical atomic-bromine Auger decay spectra are shown in panels (b), (d) and (f), respectively. The calculated spectra show total Auger yield and partial contributions of the different ionic states: $Br^{n+} \rightarrow Br^{m+}$. The experimental spectra are normalized so that the intensity of the most intense peak at 1377 eV is equal to 100.

As it can be seen from eqn (6), above the K-edge the experimentally observed population of L-holes is mainly a result of the K-hole decay, not direct photoionization. 61% of the initial K-hole states decay *via* KL X-ray emission to HBr^{+} ($2p^{-1}$) states (Note that $2s^{-1}$ cannot be reached by KL-emission), about 31% decays *via* KLL Auger decay to $HBr^{2+}(2s^{-2},2s^{-1}2p^{-1},2p^{-2})$ states and about 8% Auger decays to $HBr^{2+}(2s^{-1},2p^{-1})nl^{-1}$, where n = 3, 4. As expected, the probabilities are similar to those reported for atomic Kr in ref. 38.

As stated above, the HBr 2p core hole predominantly decays *via* LMY Auger. The corresponding transitions are indicated by the blue subsepctra in the panels (b), (d) and (f) of Fig. 9 and are related to $Br^{1+} \rightarrow Br^{2+}$ transitions in case of photoionization and $Br^{0} \rightarrow Br^{1+}$ transitions in case of resonant excitations. The Br $2p_{1/2}{}^{-1}$ core hole can also relax *via* Coster–Kronig decay to Br

($2p_{3/2}^{-1}Y^{-1}$) states. The corresponding olive subspectra are also shown in Fig. 9 and indicated by $Br_{CK}^{2+} \rightarrow Br^{3+}$ for the ionization process as well as by $Br_{CK}^{1+} \rightarrow Br^{2+}$ for resonant excitation. The differences between the olive subspectra in panels (b), (f) and (d) can be explained by the small contribution from Br $2s^{-1}$ initial states in the above K-shell and resonant $1s^{-1}\sigma^*$ cases. It should also be noted, that despite different L-hole population mechanisms, the shapes of spectra recorded above and below the K-edge are remarkably similar. The reason is that KL_2/KL_3 fluorescence ratio is nearly identical to the high energy limit of the $\sigma_{2p1/2}/\sigma_{2p3/2}$ photoionization ratio, and the fact that the main features contributing to the spectra in Fig. 9 are originating from $L_{2,3}MY$ Auger decay.

The states populated by KLX Auger decay can relax *via* further Auger decay by filling a hole in the L-shell. The contribution of this decay is displayed in Fig. 9(b) by the red subspectrum labeled $Br_{LX}^{2+} \rightarrow Br^{3+}$ and in Fig. 9(f) by the red subspectrum labeled $Br_{LX}^{1+} \rightarrow Br^{2+}$. As discussed above, the main contributions originate from the case X = L, *i.e.* they are a result of a KLL Auger decay. Note that LY, initial states of the $Br_{LX}^{2+} \rightarrow Br^{3+}$ or $Br_{LX}^{1+} \rightarrow Br^{2+}$ subspectrum might be also partly populated by the Coster–Kronig decay of Br $2p_{1/2}^{-1}$ states, however, their contributions are minor.

The experimental Auger energy line positions of the HBr molecule produced by singly ionized K and L-shells are found to be centered around the calculated neutral atomic-Br Auger spectra as shown in Fig. 2, and Fig. 9(a and c). The reason can be understood from the fact that the deep core orbitals are atomic-like because of the small difference in the electronegativity between H and Br atoms as discussed in Section 5. However, the Auger energies originating from the decay of the $1s^{-1}\sigma^*$ resonance displayed in Fig. 9 panel (e) are found to be in agreement with calculated resonant atomic-Br ($1s^{-1}4p$) Auger spectrum displayed in the Fig. 9 panel (f). At these times scales (hundreds of attoseconds), the agreement is coincidental, see Section 6.2.

7 Conclusions

A detailed study of the Br $1s^{-1}$ resonant excitations and ionization of HBr and of the subsequent two first steps of the Auger decay, namely the relaxation of K and L-holes, has been performed with state-of-the-art experimental resolution. Complementary relativistic multiconfigurational Dirac–Fock calculations for atomic Br and HBr molecule have been performed.

We presented an analysis of the partial electron yield photoabsorption spectrum in the energy range from 13 460 to 13 490 eV. The analysis allowed us to extract precise excitation energies of the $1s^{-1}\sigma^*$ and $1s^{-1}5p$ resonances. Moreover, from this and analysis of the Br 1s photoelectron spectrum, a value of 2.40(12) eV was derived for the lifetime broadening. From the fit analysis of the normal KLL Auger spectrum the Auger energies, the relative intensities and the DCH lifetime widths of $2s^{-2}$, $2s^{-1}2p^{-1}$ and $2p^{-2}$ have been derived. The 2s level $\Gamma_{2s^{-2}} \cong 2{\cdot}\Gamma_{2s^{-1}}$ was found as expected for deep core levels. For the 2p level the ratio turned out to be $\cong$2.4, which is between the values of 2 expected for deep core levels and $\cong$3 observed for shallow core levels. Finally, different lifetime broadenings were found for the $2s^{-1}2p^{-1}(^1P)$ state and the $2s^{-1}2p^{-1}(^3P)$ states.

The analysis of the resonant Auger spectra as a function of the photon energy provides evidence of strong repulsive character of the $1s^{-1}\sigma^*$ state due to the antibonding character of the σ^* orbital. The analysis of the kinetic energy and linewidth of the $1s^{-1}\sigma^* \rightarrow 2p^{-2}\sigma^*(^1D_2)$ transition shows anomalous dispersion (S-shape) and line narrowing as a function of the photon energy. This finding is interpreted as a signature of ultrafast nuclear dynamics. The anomalous dispersion and the linewidth narrowing were fitted with the aid of a simplified Kramers–Heisenberg formula, and the HBr $2p^{-2}$ DCH lifetime has been extracted and found to be comparable to the value obtained from the analysis of the normal KLL Auger spectrum. The HBr $2p^{-2}\sigma^*$ potential energy curve has been reconstructed, and its slope at the equilibrium distance of the ground state was estimated to be -13.60 eV Å^{-1}.

Finally, we presented an analysis of the L-shell Auger spectra measured with photon energies below and above 13.482 keV, *i.e.* the Br 1s ionization energy as well as on top of the $1s \rightarrow \sigma^*$ resonance. The latter two spectra represent predominately the second step of the decay cascade subsequent to Br 1s excitation or ionization. Below threshold only singly ionized L-hole initial states are produced by direct ionization. Above threshold $L_{2,3}$ holes in singly ionized HBr are induced by KL X-ray emission and L-holes in doubly ionized HBr by the KLX Auger processes; the same processes lead in case of a resonant $1s \rightarrow \sigma^*$ excitation to L-holes in neutral and singly ionized HBr, respectively. The main differences of the intensities measured below threshold, above threshold and on the resonance are related to the population of the L_1-hole in singly ionized HBr. For the Br $1s^{-1}$ core hole the KL-emission rate is larger than the Auger emission rate with a ratio of 61 to 39%. The analysis of the Auger kinetic energy peak positions resulting from the deep core-excited and ionized $1s^{-1}\sigma^*$, $1s^{-1}5p$ and $1s^{-1}$ states shows mainly decays *via* molecular Auger spectator/participator processes, due to the short lifetime of the states, in comparison to the nuclear dynamics.

Author contributions

M. S. and T. M. elaborated the research plan, T. M., O. T., R. G., L. J., I. I., D. K., S. K., Y. A., D. C., R. P., M. N. P., and M. S., participated and performed the measurement, N. B. K. J, T. M., M. P., and R. P performed the data analysis, N. B., K. J., and M. H., performed the theoretical calculations, N. B, K. J., R. P., and M. N. P., wrote the paper and all authors discussed the results and commented on the manuscript.

Conflicts of interest

There are no conflicts of interest to declare.

Acknowledgements

This project has received funding from the European Unions's Horizon 2020 research and innovation programme under Marie Skoldowska-Curie agreement no. 713606. Academy of Finland is acknowledged for funding. Experiments were performed on GALAXIES beamline at SOLEIL Synchrotron, France (Proposal No. 99170136).

References

1 D. Céolin, J. Ablett, D. Prieur, T. Moreno, J.-P. Rueff, T. Marchenko, L. Journel, R. Guillemin, B. Pilette and T. Marin, *et al.*, *J. Electron Spectrosc. Relat. Phenom.*, 2013, **190**, 188–192.

2 J.-P. Rueff, J. Ablett, D. Céolin, D. Prieur, T. Moreno, V. Balédent, B. Lassalle-Kaiser, J. Rault, M. Simon and A. Shukla, *J. Synchrotron Radiat.*, 2015, **22**, 175–179.

3 M. Simon, R. Püttner, T. Marchenko, R. Guillemin, R. K. Kushawaha, L. Journel, G. Goldsztejn, M. N. Piancastelli, J. M. Ablett and J.-P. Rueff, *et al.*, *Nat. Commun.*, 2014, **5**, 1–5.

4 M. N. Piancastelli, T. Marchenko, R. Guillemin, L. Journel, O. Travnikova, I. Ismail and M. Simon, *Rep. Prog. Phys.*, 2019, **83**, 016401.

5 M. Oura, T. Gejo, K. Nagaya, Y. Kohmura, K. Tamasaku, L. Journel, M. N. Piancastelli and M. Simon, *New J. Phys.*, 2019, **21**, 043015.

6 P. Erman, I. Bergström, Y. Chu and G. Emery, *Nuclear Phys.*, 1965, **62**, 401–409.

7 B. M. Kincaid and P. Eisenberger, *Phys. Rev. Lett.*, 1975, **34**, 1361–1364.

8 P. D'Angelo, A. Di Cicco, A. Filipponi and N. V. Pavel, *Phys. Rev. A: At., Mol., Opt. Phys.*, 1993, **47**, 2055–2063.

9 S. Southworth, R. Dunford, E. Kanter, B. Krässig, L. Young, L. LaJohn and R. Pratt, *Radiat. Phys. Chem.*, 2006, **75**, 1574–1577.

10 R. Hauko, J. Padežnik Gomilšek, A. Kodre, I. Arčon and G. Aquilanti, *Phys. Rev. A: At., Mol., Opt. Phys.*, 2019, **99**, 062501.

11 P. Morin and I. Nenner, *Phys. Rev. Lett.*, 1986, **56**, 1913.

12 O. Björneholm, S. Sundin, S. Svensson, R. R. T. Marinho, A. Naves de Brito, F. Gel'mukhanov and H. Ågren, *Phys. Rev. Lett.*, 1997, **79**, 3150–3153.

13 R. Feifel, F. Burmeister, P. Sałek, M. N. Piancastelli, M. Bässler, S. L. Sorensen, C. Miron, H. Wang, I. Hjelte, O. Björneholm, A. Naves de Brito, F. K. Gel'mukhanov, H. Ågren and S. Svensson, *Phys. Rev. Lett.*, 2000, **85**, 3133–3136.

14 F. Gel'mukhanov and H. Ãgren, *Phys. Rep.*, 1999, **312**, 87–330.

15 O. Travnikova, T. Marchenko, G. Goldsztejn, K. Jänkälä, N. Sisourat, S. Carniato, R. Guillemin, L. Journel, D. Céolin and R. Püttner, *et al.*, *Phys. Rev. Lett.*, 2016, **116**, 213001.

16 O. Travnikova, N. Sisourat, T. Marchenko, G. Goldsztejn, R. Guillemin, L. Journel, D. Céolin, I. Ismail, A. Lago and R. Püttner, *et al.*, *Phys. Rev. Lett.*, 2017, **118**, 213001.

17 T. Marchenko, G. Goldsztejn, K. Jänkälä, O. Travnikova, L. Journel, R. Guillemin, N. Sisourat, D. Céolin, M. Žitnik and M. Kavčič, *et al.*, *Phys. Rev. Lett.*, 2017, **119**, 133001.

18 H. Aksela, S. Aksela, M. Ala-Korpela, O. Sairanen, M. Hotokka, G. Bancroft, K. Tan and J. Tulkki, *Phys. Rev. A: At., Mol., Opt. Phys.*, 1990, **41**, 6000.

19 H. Aksela, S. Aksela, M. Hotokka, A. Yagishita and E. Shigemasa, *J. Phys. B: At., Mol. Opt. Phys.*, 1992, **25**, 3357.

20 I. Hjelte, M. Piancastelli, R. Fink, O. Björneholm, M. Bässler, R. Feifel, A. Giertz, H. Wang, K. Wiesner and A. Ausmees, *et al.*, *Chem. Phys. Lett.*, 2001, **334**, 151–158.

21 O. Björneholm, M. Bässler, A. Ausmees, I. Hjelte, R. Feifel, H. Wang, C. Miron, M. Piancastelli, S. Svensson and S. Sorensen, *et al.*, *Phys. Rev. Lett.*, 2000, **84**, 2826.

22 I. Hjelte, M. Piancastelli, C. M. Jansson, K. Wiesner, O. Björneholm, M. Bässler, S. Sorensen and S. Svensson, *Chem. Phys. Lett.*, 2003, **370**, 781–788.

23 P. Morin and C. Miron, *J. Electron Spectrosc. Relat. Phenom.*, 2012, **185**, 259–266.

24 L. Avaldi, G. Dawber, R. Camilloni, G. King, M. Roper, M. Siggel, G. Stefani and M. Zitnik, *J. Phys. B: At., Mol. Opt. Phys.*, 1994, **27**, 3953.

25 M. Breinig, M. H. Chen, G. E. Ice, F. Parente, B. Crasemann and G. S. Brown, *Phys. Rev. A: At., Mol., Opt. Phys.*, 1980, **22**, 520.

26 H. J. A. Jensen, R. Bast, T. Saue, L. Visscher, V. Bakken, K. G. Dyall, S. Dubillard, U. Ekström, E. Eliav, T. Enevoldsen, E. Faßhauer, T. Fleig, O. Fossgaard, A. S. P. Gomes, T. Helgaker, J. Henriksson, M. Iliaš, C. R. Jacob, S. Knecht, S. Komorovský, O. Kullie, J. K. Lærdahl, C. V. Larsen, Y. S. Lee, H. S. Nataraj, M. K. Nayak, P. Norman, G. Olejniczak, J. Olsen, Y. C. Park, J. K. Pedersen, M. Pernpointner, R. di Remigio, K. Ruud, P. Sałek, B. Schimmelpfennig, A. Shee, J. Sikkema, A. J. Thorvaldsen, J. Thyssen, J. van Stralen, S. Villaume, O. Visser, T. Winther and S. Yamamoto, *DIRAC, a relativistic ab initio electronic structure program. Release DIRAC16*, 2016. See http://www.diracprogram.org.

27 K. G. Dyall, *Theor. Chem. Acc.*, 2006, **115**, 441–447.

28 P. Bunker, *J. Mol. Spectrosc.*, 1972, **42**, 478–494.

29 P. Jönsson, X. He, C. F. Fischer and I. Grant, *Comput. Phys. Commun.*, 2007, **177**, 597–622.

30 J. Niskanen, K. Jänkälä, M. Huttula and A. Föhlisch, *J. Chem. Phys.*, 2017, **146**, 144312.

31 S. Fritzsche, *Comput. Phys. Commun.*, 2012, **183**, 1525–1559.

32 M. F. Gu, *Can. J. Phys.*, 2008, **86**, 675–689.

33 R. Püttner, M. Domke, K. Schulz, A. Gutiérrez and G. Kaindl, *J. Phys. B: At., Mol. Opt. Phys.*, 1995, **28**, 2425.

34 R. Püttner, Y.-F. Hu, E. Nommiste, G. Bancroft and S. Aksela, *Phys. Rev. A: At., Mol., Opt. Phys.*, 2002, **65**, 032513.

35 A. L. Allred, *J. Inorg. Nucl. Chem.*, 1961, **17**, 215–221.

36 G. B. Armen, J. Tulkki, T. Aberg and B. Crasemann, *Phys. Rev. A: At., Mol., Opt. Phys.*, 1987, **36**, 5606.

37 M. O. Krause and J. Oliver, *J. Phys. Chem. Ref. Data*, 1979, **8**, 329–338.

38 N. Boudjemia, K. Jänkälä, R. Püttner, T. Gejo, L. Journel, Y. Kohmura, M. Huttula, M. N. Piancastelli, M. Simon and M. Oura, *Phys. Rev. A: At., Mol., Opt. Phys.*, 2020, **101**, 053405.

39 V. Carravetta, H. Ågren, D. Nordfors and S. Svensson, *Chem. Phys. Lett.*, 1988, **152**, 190–195.
40 V. Schmidt, *Electron spectrometry of atoms using synchrotron radiation*, Cambridge University Press, 1997, p. 73.
41 R. Guillemin, S. Sheinerman, R. Püttner, T. Marchenko, G. Goldsztejn, L. Journel, R. Kushawaha, D. Céolin, M. N. Piancastelli and M. Simon, *Phys. Rev. A: At., Mol., Opt. Phys.*, 2015, **92**, 012503.
42 G. Goldsztejn, T. Marchenko, R. Püttner, L. Journel, R. Guillemin, S. Carniato, P. Selles, O. Travnikova, D. Céolin and A. Lago, *et al.*, *Phys. Rev. Lett.*, 2016, **117**, 133001.
43 M. Žitnik, R. Püttner, G. Goldsztejn, K. Bučar, M. Kavčič, A. Mihelič, T. Marchenko, R. Guillemin, L. Journel and O. Travnikova, *et al.*, *Phys. Rev. A: At., Mol., Opt. Phys.*, 2016, **93**, 021401.
44 R. Püttner, G. Goldsztejn, D. Céolin, J.-P. Rueff, T. Moreno, R. K. Kushawaha, T. Marchenko, R. Guillemin, L. Journel and D. W. Lindle, *et al.*, *Phys. Rev. Lett.*, 2015, **114**, 093001.
45 R. Püttner, D. Céolin, R. Guillemin, R. K. Kushawaha, T. Marchenko, L. Journel, M. N. Piancastelli and M. Simon, *Phys. Rev. A: At., Mol., Opt. Phys.*, 2016, **93**, 042501.
46 R. Püttner, P. Holzhey, M. Hrast, M. Žitnik, G. Goldsztejn, T. Marchenko, R. Guillemin, L. Journel, D. Koulentianos, O. Travnikova, M. Zmerli, D. Céolin, Y. Azuma, S. Kosugi, A. Föhlisch, M. N. Piancastelli and M. Simon, to be submitted, 2020.
47 D. Céolin, T. Marchenko, R. Guillemin, L. Journel, R. K. Kushawaha, S. Carniato, S.-M. Huttula, J. P. Rueff, G. B. Armen, M. N. Piancastelli and M. Simon, *Phys. Rev. A: At., Mol., Opt. Phys.*, 2015, **91**, 022502.
48 G. Goldsztejn, T. Marchenko, D. Céolin, L. Journel, R. Guillemin, J.-P. Rueff, R. K. Kushawaha, R. Püttner, M. N. Piancastelli and M. Simon, *Phys. Chem. Chem. Phys.*, 2016, **18**, 15133–15142.
49 R. Püttner, K. Jänkälä, R. K. Kushawaha, T. Marchenko, G. Goldsztejn, O. Travnikova, R. Guillemin, L. Journel, I. Ismail, B. Cunha de Miranda, A. F. Lago, D. Céolin, M. N. Piancastelli and M. Simon, *Phys. Rev. A: At., Mol., Opt. Phys.*, 2017, **96**, 022501.
50 H. A. Kramers and W. Heisenberg, *Z. Phys.*, 1925, **31**, 681–708.
51 J. Campbell and T. Papp, *At. Data Nucl. Data Tables*, 2001, **77**, 1–56.
52 S. J. Blanksby and G. B. Ellison, *Acc. Chem. Res.*, 2003, **36**, 255–263.
53 L. O. Werme, T. Bergmark and K. Siegbahn, *Phys. Scr.*, 1972, **6**, 141–150.
54 A. Kovalík, V. Gorozhankin, A. Novgorodov, A. Minkova, M. Mahmoud and M. Ryšavý, *J. Electron Spectrosc. Relat. Phenom.*, 1992, **58**, 49–66.
55 M. N. Piancastelli, K. Jänkälä, L. Journel, T. Gejo, Y. Kohmura, M. Huttula, M. Simon and M. Oura, *Phys. Rev. A: At., Mol., Opt. Phys.*, 2017, **95**, 061402.
56 N. Boudjemia, K. Jänkälä, T. Gejo, K. Nagaya, K. Tamasaku, M. Huttula, M. N. Piancastelli, M. Simon and M. Oura, *Phys. Chem. Chem. Phys.*, 2019, **21**, 5448–5454.